pH-triggered intracellular release from actively targeting polymer micelles

Xing Guo [a], Chunli Shi [b], Jie Wang [a], Shubin Di [a], Shaobing Zhou [a,*]

[a] Key Laboratory of Advanced Technologies of Materials, Ministry of Education, School of Materials Science and Engineering, Southwest Jiaotong University, Chengdu 610031, China
[b] School of Life Science and Engineering, Southwest Jiaotong University, Chengdu 610031, China

ARTICLE INFO

ABSTRACT

Chemotherapy is widely applied to treat cancer patients but its application is limited due to the systemic toxicity and low efficacy. Nanocarrier system, which is capable of delivering their toxic cargos specifically into cancer cells and then greatly overcomes these disadvantages, has drawn a broad attention. Here we developed a drug-conjugated micelle for a better drug delivery in which folic acid was attached to the DOX-conjugated poly(ethylene glycol)-poly(ε-caprolactone) to target tumor; DOX was further connected with a hydrazone linker (FA-hyd) for a pH-triggered drug release. Comparing to other DOX-conjugated micelles either linked with carbamate (FA-cbm) or lacking FA(m-hyd), the developed FA-hyd demonstrated excellent biocompatibility; When analyzed with Alamar blue assays, flow cytometry and confocal laser scanning microscopy (CLSM), the pH-sensitive FA-functionalized DOX-conjugated micelles presented much better efficiency of cellular uptake and higher cytotoxicity to tumor cells. In vivo pharmacokinetics and biodistribution studies indicated that FA-hyd micelles significantly prolonged the blood circulation time of drug and enriched drug into the tumors rather than normal tissues. In vivo antitumor activity demonstrated that FA-hyd micelles had the highest safety to body and the best therapeutic efficacy to tumors. Therefore, this drug delivery system is deemed as a potential nanocarrier for cancer therapy.

1. Introduction

Drug delivery is one of the most promising biomedical applications of nanotechnology in cancer chemotherapy [1]. An ideal nanocarrier holds the features for a better therapy but with minimal side effects, such as a long circulation half-life in the blood and effective delivery of encapsulated therapeutic agents [2]. A number of nanocarriers have been developed by using various organic or inorganic materials [3–6] and some nanocarriers have been successfully used for the controlled delivery of water-insoluble drugs in cancer therapy [3,7–13]. Micelles with a core—shell architecture, which are formed through self-assembly of amphiphilic block copolymers, have small size (usually < 100 nm), therefore can accumulate spontaneously in solid tumors through the well-known enhanced permeability and retention (EPR) effect [14,15]. However, the lack of specific targeting to tumor cells and poor cellular

internalization of the micelles reduces the therapeutic efficacy of the encapsulated agents while induces multiple drug resistance as well as high toxicity against normal cells [16–18].

To further improve delivery efficiency and cancer-targeting specificity, the actively targeting strategy has been developed by utilizing ligands to generate specific interaction between micelles and molecular biomarkers on tumor cell membranes [19–21]. To date, the employed targeting ligands are mainly including antibodies, aptamers and small molecules [3,22]. The actively targeting micelles can specifically recognize the corresponding receptors which are abundantly exist on the surfaces of tumor cell, thus are effectively internalized by tumor cells via ligand/receptor-mediated endocytosis [4,23,24]. For instance, since many cancer cells yet rarely normal cells are highly expressing folate receptor (FR), folic acid (FA) is often employed to functionalize the micelles for an active tumor targeting and thus to effectively enhance therapeutic efficacy both in vitro and in vivo [25–27]. In addition, anticancer drugs encapsulated with their nanocarriers also need to be released in the cellular compartments such as the cytoplasm or nucleus in a timely manner after entering the cells, thus exerting their high therapeutic efficiency to solid tumors [8,28]. Currently, the design

* Corresponding author. Tel.: +86 28 87634023; fax: +86 28 87634649.
E-mail addresses: shaobingzhou@swjtu.edu.cn, shaobingzhou@hotmail.com
(S. Zhou).

and engineering of nanocarriers that can execute multiple tasks simultaneously is still a challenge in cancer research.

To address this challenge, the environment-responsive polymer micelles have been developed by employing the external stimuli. These stimuli cause destabilization of micelles in a specially controlled manner, thus increasing the selectivity and efficiency of drug delivery [6,17,29,30]. Of these stimuli, pH-responsiveness is the most frequently used [7,31–35]. The application of pH-sensitivity is based on the fact that pH values vary sharply in different tissues and cellular compartments. The increased aerobic glycolysis in cancer cells leads to the lower extracellular pH of cancer cells (pH 6.5–7.2) than that in normal tissues [36,37]. In addition, the pH value of early endosome in cells is around 5–6 while the late lysosome is much more acidic compartment (pH 4–5) [38,39].

In this study, we present a polymeric micelle system for tumor targeting and pH-triggered drug release (Scheme 1). The anticancer drug, DOX, is chemically conjugated to the polymer backbone via pH-responsive linkers to form so-called "polymeric prodrugs" [40–42]. FA bared onto the surface of the nanocarriers facilitates the endocytosis by the FR over-expressing tumor cells. Once the polymeric prodrugs are internalized by the tumor cells and included into the endo/lysosomes, the hydrazone linkages are ruptured due to the acidic microenvironment and DOX is released from polymer. It is anticipated that the combination of the FR mediated targeting and the pH-triggered release of payloads can greatly enhance the drug delivery efficiency and therapeutic outcome in vivo application.

2. Materials and methods

2.1. Materials

Poly(ethylene glycol) (PEG, $M_n = 2$ kDa) and folic acid (FA) were purchased from KeLong Chemicals (Chengdu, China). PEG was purified before use. ε-Caprolactone (ε-CL; Aldrich) was dried over CaH_2 overnight and distilled at reduced pressure before use. Doxorubicin hydrochloride (DOX·HCl) was purchased from Zhejiang Hisun Pharmaceutical Co., Ltd. (China), and Doxorubicin (DOX) was obtained by dehydrochlorination. 1-Ethyl-3-(3-dimethyllaminopropyl) carbodiimide hydrochloride (EDC·HCl) and N-hydroxysuccinimide (NHS) were purchased from Sigma chemicals (St. Louis, MO, USA). All the other chemicals were purchased from commercial supplier and used without further purification.

2.2. Cell lines and culture conditions

The human nasopharyngeal epidermoid carcinoma cell line KB and human lung epithelial tumor cell line A549 were obtained from Sichuan University (China). Cells were grown as adherent cultures and maintained in RPMI 1640 added with 10% fetal bovine serum at 37 °C and 5% CO_2 under fully humidified conditions.

2.3. Animals

Female BALB/c mice (20 ± 2 g), approved by the Institutional Animal Care and Use Committee of Sichuan University, were feed at the condition of 25 °C and 55% of humidity. All animal experiments were carried out in compliance with guidelines.

2.4. Synthesis of folic acid-attached polymeric prodrugs with conjugated DOX

2.4.1. Synthesis of CDI-activated PEG (CDI-PEG-OH)
N,N′-Carbonyldiimidazole (CDI) (0.81 g, 5 mmol) was dissolved in dry dichloromethane (15 mL) and added dropwise into dichloromethane (15 mL) solution of the purified PEG (10 g, 5 mmol). The mixture was kept stirring at 25 °C under nitrogen atmosphere for 6 h. The excess dichloromethane was removed by
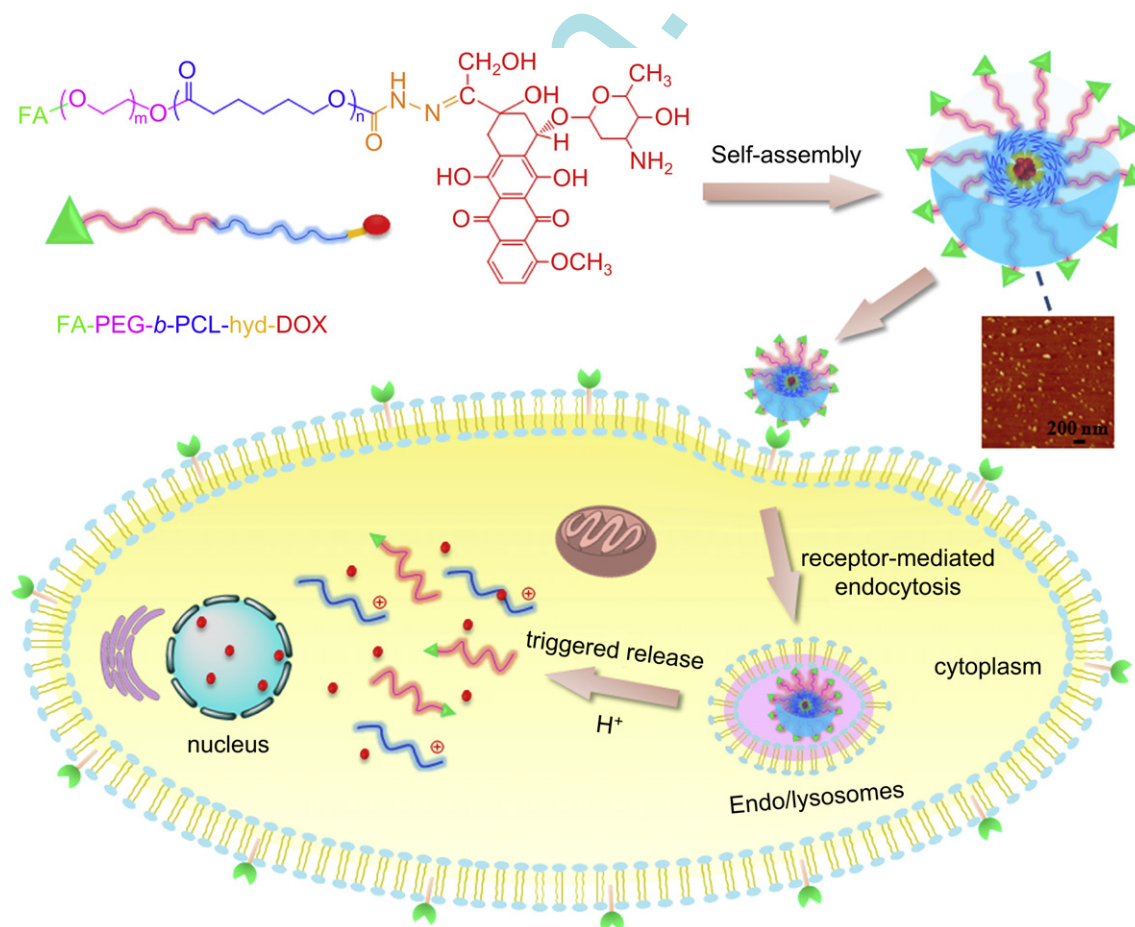
FA-PEG-b-PCL-hyd-DOX

Scheme 1. Illustration of polymeric-drug conjugated micelles based on FA-PEG-b-PCL-hyd-DOX for receptor-mediated endocytosis and efficient pH-triggered release, and AFM image of the micelles.

rotary evaporator, and the concentrated solution was poured into an excess amount of ethyl ether to precipitate the product. This process was repeated three times to remove unreacted CDI. The CDI-PEG-OH was dried under vacuum to obtain the white powder (yield: 91.5%) [43].

2.4.2. Synthesis of CDI-PEG-PCL copolymer (CDI-PECL)

CDI-PEG-PCL was synthesized through ring-opening polymerization (ROP) of ε-CL initiated by CDI-PEG-OH in the presence of SnCl₂ as the catalyst. Briefly, pre-weighed CDI-PEG-OH (8.58 g, 4 mmol), ε-CL (13.68 g, 120 mmol) monomer and SnCl₂ (1 wt%) were quickly added to a 150 mL round-bottom flask with a stopcock which was preheated to remove the moisture. Then the flask was degassed under vacuum for 6 h with continuous stirring. After that, the ring-opening polymerization reaction was carried out at 140 °C for another 6 h. The copolymer was obtained by dissolving the viscous material into a little amount of dichloromethane and precipitated in excess cold ethanol, and collected by centrifugation. The resultant light yellow product was dried under vacuum to remove ethanol completely (yield: 88.6%).

2.4.3. Synthesis of amino-terminated PEG-PCL (NH₂-PECL) [44]

The anhydrous dichloromethane solution of CDI-PECL-OH (16.5 g, 3 mmol) was added dropwise into 15 mL of 1,2-ethylenediamine at 25 °C. The mixture was then reacted overnight. The excess dichloromethane and unreacted 1,2-ethylenediamine were removed by rotary evaporation. The concentrated viscous mixture was poured into an excess amount of cold ethanol to precipitate the product. NH₂-PEG-PCL was dried under a vacuum dehydration and collected as yellow powder (yield: 74.9%).

2.4.4. Synthesis of folate-conjugated PEG-PCL (FA-PECL)

Folic acid (0.88 g, 2 mmol), NHS (0.23 g, 2 mmol) and EDC·HCl (0.42 g, 2.2 mmol) were dissolved in 100 mL DMSO. The mixture was stirred at 25 °C under nitrogen atmosphere in the dark overnight. Then, NH₂-PEG-PCL (10.96 g, 2 mmol) and several drop of triethylamine were added, and the mixture was reacted for another 24 h in the same condition. DMSO and unreacted folic acid were removed by dialysis against deionized water for 3 days. FA-PEG-PCL was collected by lyophilization (yield: 89.3%).

2.4.5. Synthesis of NPC-activated FA-PECL (FA-PECL-NPC)

The hydroxyl group of FA-PECL-OH was activated by p-nitrophenyl chloroformate. Briefly, FA-PECL (6.6 g, 1 mmol) and several drop of triethylamine were dissolved in 60 mL dry dichloromethane and stirred at 0 °C. The dichloromethane solution of p-nitrophenyl chloroformate (0.2 g, 1 mmol) was added dropwise into the reaction mixture and stirred at 0 °C for 2 h and at 25 °C for another 24 h under nitrogen atmosphere. FA-PECL-NPC was obtained by concentrating the mixture and precipitating into cold ethanol to give the yellow powder (yield: 81.6%).

2.4.6. Synthesis of hydrazine monohydrate-terminated FA-PECL (FA-PECL-hyd)

FA-PECL-NPC (2.0 g, 0.3 mmol) was dissolved in 20 mL dichloromethane and reacted with hydrazine monohydrate (0.14 mL, 3 mmol). The solution was reacted for 24 h at 25 °C. The resultant solution was concentrated and poured into cold ethanol to precipitate FA-PECL-hyd, and the product was dried under vacuum (yield: 75.9%).

2.4.7. Synthesis of DOX-conjugated FA-PECL by a hydrazone linker (FA-PECL-hyd-DOX) [45]

FA-PECL-hyd (100 mg, 0.017 mmol) and DOX (9.6 mg, 0.017 mmol) were dissolved in 10 mL anhydrous dimethylformamide. The mixture was reacted in the presence of a drop of triethylamine at 25 °C under nitrogen atmosphere for 48 h. The resultant solution was dialyzed (MWCO 1000) against deionized water for 24 h to remove DMF and unreacted DOX. FA-PECL-hyd-DOX was obtained by lyophilization (yield: 86.2%).

2.4.8. Synthesis of DOX-conjugated FA-PECL by a carbamate linker (FA-PECL-cbm-DOX)

FA-PECL-NPC (100 mg, 0.015 mmol) and DOX (8.5 mg, 0.015 mmol) were dissolved in 10 mL anhydrous dimethylformamide. The mixture was reacted in the presence of a drop of triethylamine at 25 °C under nitrogen atmosphere for 48 h. The resultant solution was dialyzed (MWCO 1000) against deionized water for 24 h to remove DMF and unreacted DOX. FA-PECL-cbm-DOX was obtained by lyophilization (yield: 81.8%).

2.5. Preparation of blank and DOX-conjugated micelles

The blank and DOX-conjugated micelles were fabricated by the solvent evaporation method. Briefly, the freeze-dried powder (1 mg) of FA-PECL, FA-PECL-hyd-DOX or FA-PECL-cbm-DOX was dissolved in 5 mL of tetrahydrofuran (THF) as a good solvent, and then the solution was added dropwise using a disposable syringe (21 gauge) under high-speed stirring to 10 mL ultrapurified water as a selective solvent. The micelle solution was filtered through a 450 nm syringe filter before size and morphology detection.

2.6. Characterizations

¹H NMR spectra were obtained on a Bruker AM 300 apparatus. DMSO-d₆, CDCl₃ or D₂O was used as a solvent according to the purpose, and Tetra-methylsilane (TMS)

was used as the internal reference. The composition of copolymer was calculated from the ¹H NMR spectrum on the basis of the already known number-averaged molecular weight of PEG. Chemical shifts are expressed in parts permillion, ppm (δ). The UV−vis absorption spectra were measured on a UV−vis spectrophotometer (UV-2550, Shimadzu, Japan).

The molecular weights of the polymers were analyzed using a gel permeation chromatography (GPC) system equipped with a Water 2695 pump and a Styragel HT4DMF column operated at 40 °C and series 2414 refractive index detector with polystyrene as a standard for calibration.

Dynamic light scattering (DLS) (ZETA-SIZER, MALVERN Nano-ZS90, Malvern, U.K) was performed to determine the mean size and size distribution of the micelles. The solutions of micelles in standard phosphate buffer or acetate buffer with desired pH values were filtered through a 450 nm syringe filter. Each measurement was carried out in triple at 25 °C, and an average value was reported.

Atomic force microscopy (AFM) (CSPM5000, Being, China) was employed to further observe the morphologies of the micelles. The AFM sample was prepared by placing a drop of micellar solution (10 μL, 1 mg/mL) on a silicon wafer, and dried in a desiccator at room temperature before AFM observation. Tapping-mode AFM was utilized to scan the sample after the sample-loaded silicon wafer was totally dried.

Fluoromax spectrometer (F-7000, Hitach, Japan) was performed to determine the critical micelle concentration (CMC) of micelles. Pyrene was used as a florescent probe. The excitation wavelength was set to 390 nm, and the fluorescence intensity was detected at 333 and 339 nm. CMC was measured from the onset of a decrease in the intensity ratio of peak at 333 nm to peak at 339 nm plotted versus the logarithm of polymer concentration.

DOX-loading content (DL) and conjugation efficiency (CE) was measured by UV−vis analysis using a UV−vis Spectrophotometer (UV-2550, Shimadzu, Japan). The preweighed freeze-dried sample was re-dissolved in DMSO. By using a pre-established calibration curve, the absorbance of DOX at 488 nm was measured to detect the DOX concentration in the solution.

2.7. pH-responsive behaviors and in vitro DOX release

GPC and ¹H NMR were used to detect the cleavage of hydrazone bond in FA-hyd. The samples were prepared by dissolving the freeze-dried micelle in 3 mL DMF (10 mg/mL) and incubated with 1 mL various pH value HCl (pH ~ 4, 5, 6) and PBS (pH ~ 7.4) for 24 h, the solutions were dried in a vacuum oven overnight at 60 °C. The samples were dissolved in DMF for GPC test at a flow rate of 1.0 mL/min. And the samples were dissolved in DMSO-d₆ for ¹H NMR detect.

In the direct assessment of DOX release from the DOX-conjugated micelle with a hydrazone linker, the freeze-dried micelle was dissolved in acetate buffer at pH 5.0 or phosphate buffer at pH 7.4 at a concentration of 0.5 mg/mL, and the fluorescence intensity was measured at different time points (0−240 min) on a Fluoromax spectrometer (F-7000, Hitach, Japan) using excitation wavelength of 505 nm, excitation slit width of 10 nm, emission slit width of 10 nm, and scanning speed of 500 nm/min.

To quantitatively determine the release rate of DOX from the micelle solutions, freeze-dried samples (10 mg each) were re-suspended in 10 mL phosphate buffered solution (PBS) at pH 7.4 or acetate buffered solution (ABS) at pH 5.0, respectively. The solutions were transferred into dialysis bags (MWCO: 1000) and immersed into 30 mL PBS or ABS in a prepared tube under a predetermined sink condition. The tubes were kept at 37 °C in a thermostated incubator with a shaking speed at 100 cycles/min. At selected time intervals from 0.5 to 48 h, 1 mL of solution outside the dialysis bag was taken out and replaced with the same volume of fresh medium. The concentration of DOX released from DOX-conjugated micelles was determined by a fluorescence spectrophotometer. The cumulative amount of released DOX was calculated, and the percentages of DOX released were plotted against time.

2.8. Biocompatibility evaluation

The biocompatibility assessment of FA-PECL blank micelle was based on hemolysis assay. In brief, 200 μL human whole blood was added into the blank micelle of saline solution with different concentrations ranged from 0.5 mg/mL to 2 mg/mL. The same volume of ultrapure water was used as the positive control, and saline was the negative control. All the samples were centrifuged to obtain the supernatants after they were incubated at 37 °C for 60 min. The absorbances of the supernatants were measured in an automated microplate spectrophotometer (ELX800 Biotek, USA) at 540 nm and then compared to a standard curve (hemoglobin concentrations ranging from 0.005 to 2.5 mg/mL). Percent hemolysis was calculated by the formula described as:

$$Hemolysis\% = \frac{As - Aneg}{Apos - Aneg} \times 100\%$$

where As, Aneg, Apos are the absorbance of the sample, the negative control and the positive control, respectively.

Coagulation measurements were evaluated by the activated partial thromboplastin time (APTT) assay, prothrombin time (PT) assay and thrombin time (TT)

assay. Firstly, platelet-poor plasma (PPP) was obtained by centrifuging the whole blood at 3000 rpm for 10 min. Then 0.5 mL PPP was added into a 24-well plate with 2 mg polymer powder inside. The plate was incubated at 37 °C for 30 min. The APTT assay was performed as follows. Briefly, 200 μL incubated PPP solutions was added into a test tube with 100 μL APTT reagent inside. Then 100 μL 0.03 M CaCl₂ solution was added after the tube was incubating at 37 °C for 5 min. The clotting time was measured by a coagulometer (Clot 1A, Innova Co.). The PT and TT assays were almost similar with the APTT assay, except that the reagent was different.

2.9. In vitro cell cytotoxicity assay

Cytotoxicity of the blank micelle and tumor cell inhibition of DOX-conjugated micelles were evaluated by Alarmar blue assays. Human nasopharyngeal epidermoid carcinoma cells (KB), lung epithelial cancer cells (A549) and osteoblasts (OB) were seeded at a density of 5×10^3 cells per well into 48-well plates with RPMI 1640 supplemented with 10% FBS. The two tumor cell lines have different levels of folate receptor (FR) expression. In particular A549 cells are FR negative (FR−) and KB cells are FR positive (FR+). The cells were cultured in the incubator at 37 °C in humidified atmosphere containing 5% CO₂ for 24 h. The medium was then replaced with fresh medium, and pre-prepared blank micelle or DOX-conjugated micelles were added to incubate with the cells. The concentration of blank micelle varied from 10 to 100 μg/mL and DOX-conjugated micelles with DOX content ranged from 0.025 to 10.0 μg/mL. After 24 h, the medium was removed, each well was rinsed with PBS, and 250 μL of Alamar Blue solution (10% Alamar Blue, 80% media 199 (Gibcos), and 10% FBS, v/v) was added and incubated for further 3 h. A sample of 200 μL of Alamar blue solution was pipetted into a 96-well plate and the plate was read in an automated microplate spectrophotometer (ELX800 Biotek, USA) at 570 nm (excitation)/600 nm (emission). The results are the mean ± standard deviation in triple.

2.10. Determination of the intracellular accumulation [46]

Two tumor cell lines with different FR expressions were selected to perform the in vitro cellular uptake of DOX-conjugated micelles. A549 and KB cells were seeded at a density of 1.0×10^5 cells per well into 6-well plates with RPMI 1640. The cells were maintained in the incubator at 37 °C in humidified atmosphere containing 5% CO₂. After 24 h, pre-prepared free DOX solution and DOX-conjugated micelle solution with a same dosage of 5 ug/mL DOX were added into 6-well plate. After 3 h, the medium was removed and each well was rinsed with PBS. The cells were then fixed with 2.5% glutaraldehyde for 30 min and the cell nuclei was stained with 4′, 6-diamidino-2-phenylindole (DAPI, blue) for 3 min. The fluorescence images of free DOX, FA-hyd, FA-cbm, and m-hyd in cells were observed by an inverted fluorescence microscope (Olympus, CKX41) with a charge-coupled device camera (Imaging, Micropublisher 5.0 RTV) and a mercury lamp (Olympus, U-RFLT50).

CLSM was performed to observe the intracellular distribution of DOX. KB cells were seeded at a density of 1.0×10^5 cells per well into 6-well plates with RPMI 1640, and incubated for 2 h with PBS solutions containing DOX, FA-hyd, FA-cbm, m-hyd and FA-hyd with blocking at a DOX dose of 5 ug/mL. The medium was removed and each well was rinsed with PBS 3 times, and Lysotracker Green (Beyotime Biotech, China) was added to incubated with cells for further 0.5 h to identify the drug location inside cells. Cells were observed on a Leica Microsystems CMS Gmbh (TCS SP5, Germany), DOX and Lysotracker Green were excited at 485 and 504 nm, respectively. The emission wavelengths of DOX and Lysotracker Green are 595 and 511 nm, respectively.

2.11. In vivo and ex vivo DOX fluorescence imaging

Free DOX, DOX-conjugated micelles and PBS were injected into 4T1 tumor bearing nude mice via lateral tail vein at a dosage of 5 mg DOX/Kg body weight. The mice were then anesthetized and imaged by Maestro In-vivo Imaging System from 0.5 h to 5 h. At 5 h postinjection, the mice were sacrificed and the normal organs as well as tumors were excised for ex vivo imaging. The emission fluorescence was collected from 500 nm to 750 nm, and the 455 nm excitation filter was used.

2.12. Evaluation of pharmacokinetics and biodistribution in vivo

Free DOX and DOX-conjugated micelles solution were administered via the tail vein with a dosage of 5 mg DOX/Kg in 100 μL 0.9% NaCl. Blood samples were obtained via eyeball extirpating at selected time intervals (0.5–24 h) using a heparinized capillary tube. Blood samples were then centrifuged at 3000 rpm/min for 10 min to isolate plasma, the plasma was frozen at −20 °C until analysis. After blood collection, mice were sacrificed to collect the organs and tumors, the tissues were rinsed in buffer, weighed and frozen at −20 °C until analysis. The fluorescence of the samples was measured. Pharmacokinetic parameters such as $\tau_{1/2}$, area under the curve (AUC), volume of distribution (V_d) and clearance (CL) were calculated by fitting the blood drug pharmaceutical concentrations to a two-compartment model using EXCEL. The percent injected dose (% ID) and the percent ID per gram (% ID/g) values were calculated using the following equations:

$$\%ID = \frac{\text{Dose in blood/tissue sample}}{\text{Injected dose}} \times 100 \quad (1)$$

$$\%ID/g = \frac{\%ID}{\text{Weight of tissue(g)}} \quad (2)$$

2.13. In vivo antitumor effect studies

All surgical interventions and post-operative animal care were approved by the Institutional Animal Care and Use Committee of Sichuan University. Murine breast cancer cells 4T1 (1.0×10^6) were implanted in the right back area of the 5–6 weeks old female nude mice or Balb/c mice (20 ± 2 g) subcutaneously. Tumor volume was calculated by the following equation: Volume $= 0.5 \times a \times b^2$, where (a) and (b) are width and length of the tumor. When the tumor reached a mean size of approximately 50 mm³, treatments were carried out. The mice were randomly divided into five groups (n = 7). Free DOX, or DOX-conjugated micelles in 100 μL of 0.9% NaCl solution were injected via lateral tail vein at an interval of 2 days (0, 3, 6, 9, 12 day) at a dosage of 5 mg DOX/Kg body weight. And the same volume of 0.9% NaCl solution was injected into control group. Survival rate was analyzed by a log-rank test based on the Kaplan–Meier survival analysis by using Graphpad Prism software.

2.14. Histological examination

The mice were sacrificed and tumors were collected and fixed with 10% PBS buffered formalin for 24 h. After deparaffinization, tissue sections were stained with haematoxylin/eosin (H&E). At least five paraffin sections from each animal were used for H&E staining. The histological slices obtained were observed by optical microscopy.

3. Results and discussion

3.1. Synthesis and characterization of folic acid-attached polymeric prodrugs with conjugated DOX

Three types of polymeric prodrugs, the folic acid-attached poly(ethylene glycol)-poly(ε-caprolactone) (PECL) conjugated with DOX via a hydrazone linker (FA-hyd) or a carbamate linker (FA-cbm), and mPECL-hyd-DOX (m-hyd) without FA were synthesized through a series reactions as shown in Fig. 1. ¹H NMR confirmed the chemical structures of the intermediates and end products (Supporting Information, Fig. S2). Besides, from ¹H NMR analysis, we obtained the composition of the copolymer with 2 kDa for PEG and 3.5 kDa for PCL, which is in line with Gel permeation chromatography (GPC) measurement, and there existed a narrow molecular weight distribution (PDI: 1.09) (Supporting Information, Table S1). According to UV–vis absorbance at 488 nm, the DOX content in the polymer-drug conjugates was 4.57 wt.% for FA-hyd and 4.79 wt.% for FA-cbm, corresponding to a conjugation efficiency of 50.27% and 52.69%, respectively (Supporting Information, Table S2).

3.2. Preparation and characterization of the micelles

We then constructed our drug delivery system from the resultant copolymers. All of the micelles appeared to be discrete and round nanoparticles under Atomic force microscopy (AFM) (Fig. S2A–C). The dynamic light scattering (DLS) measurement showed that the average diameter of DOX-conjugated micelles was 70.9 nm for FA-hyd, and 86.6 nm for FA-cbm. The blank FA-PECL micelles were a little smaller than drug-conjugated micelles as measured by AFM and DLS (Fig. S2D–F). The CMC values of these micelles were 1.78×10^{-3} mg/mL for FA-PECL, 1.28×10^{-3} mg/mL for FA-hyd, and 1.21×10^{-3} mg/mL for FA-cbm, respectively (Fig. S3). The low CMC values demonstrated that all of the micelles were very stable even when diluted within the body. To prove the core–shell structure of micelles, ¹H NMR of the conjugates with a solvent of D₂O was performed. As shown in Fig. S4, the characteristic peaks of hydrophobic PCL block and DOX were almost disappeared, and those of folic acid and PEG were significantly enhanced. However, all of the resonance peaks for folic acid, PEG,
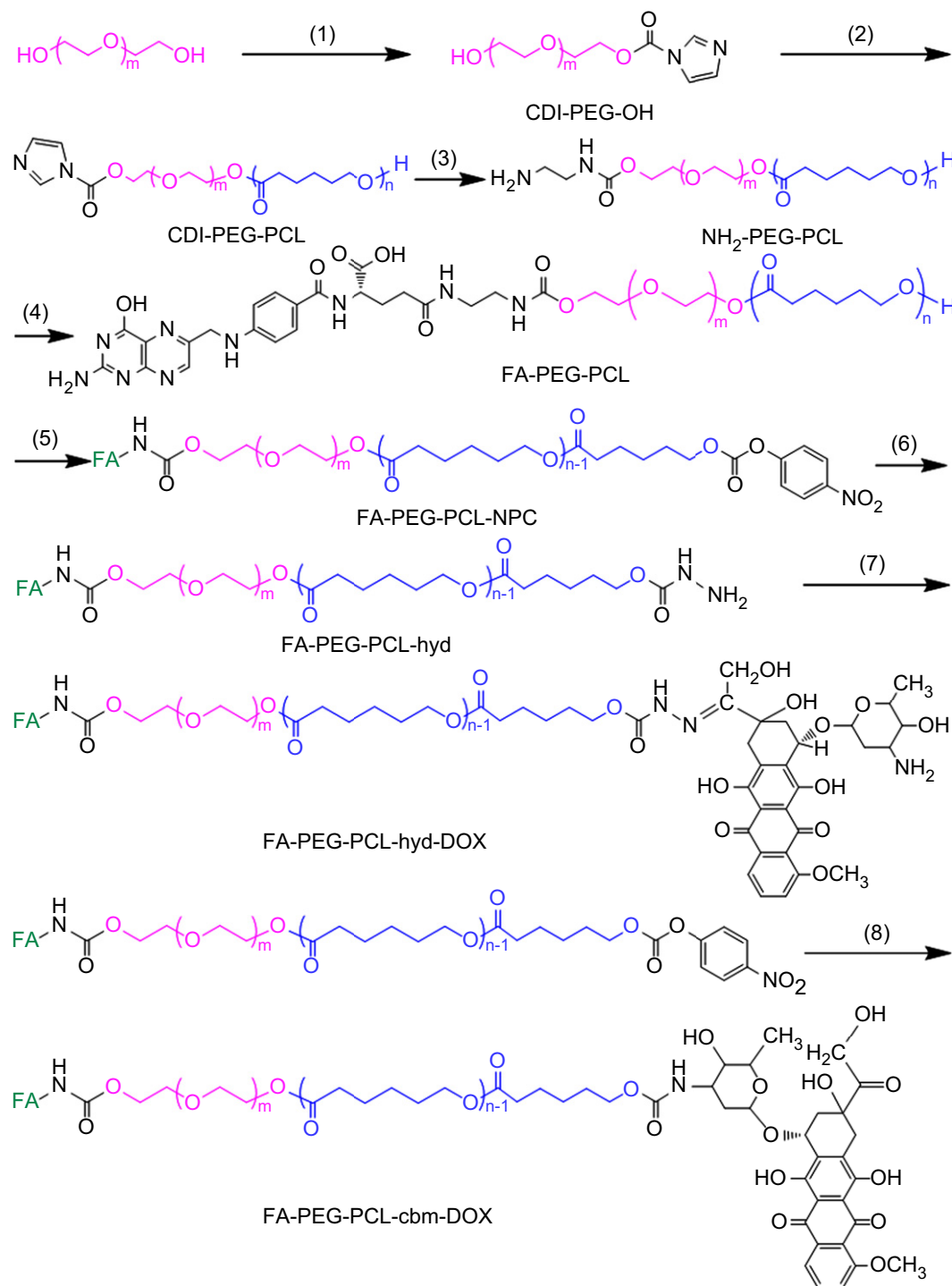
Fig. 1. Synthesis of folic acid-attached poly(ethylene glycol)-poly(ε-caprolactone) with conjugated DOX by a hydrazone linker (FA-PEG-PCL-hyd-DOX) or by a carbamate linker (FA-PEG-PCL-cbm-DOX). (1) N,N′-carbonyldiimidazole (CDI), dichloromethane (CH₂Cl₂); (2) ε-caprolactone (ε-CL), stannous chloride (SnCl₂); (3) 1,2-ethylenediamine, dichloromethane; (4) folic acid, N-hydroxysuccinimide (NHS), 1-(3-Dimethylaminopropyl)-3-ethylcarbodiimide hydrochloride (EDC), triethylamine (TEA), dimethyl sulfoxide (DMSO); (5) p-nitrophenyl chloroformate, triethylamine, dichloromethane; (6) hydrazine monohydrate, dichloromethane; (7) doxorubicin, triethylamine, N,N′-dimethylformamide (DMF); (8) doxorubicin, triethylamine, N,N′-dimethylformamide.

PCL and DOX segments were detected in DMSO-d_6 (Fig. S1F, G). These results strongly indicate that DOX-conjugated copolymers were successfully self-assembled into the core–shell structured micelles in aqueous solution, in which DOX molecules were packed in the core through hydrophobic interaction, while the folic acid ligands were exposed outside of the shell.

3.3. pH-responsive behaviors and in vitro DOX release

To demonstrate that the hydrazone bonds are cleaved in the acidic environment (Fig. 2A) [7], we incubated FA-hyd under pH ∼ 7.4 for 24 h. GPC curves showed a single peak of the copolymer. However, a new peak with molecular weight of hundreds
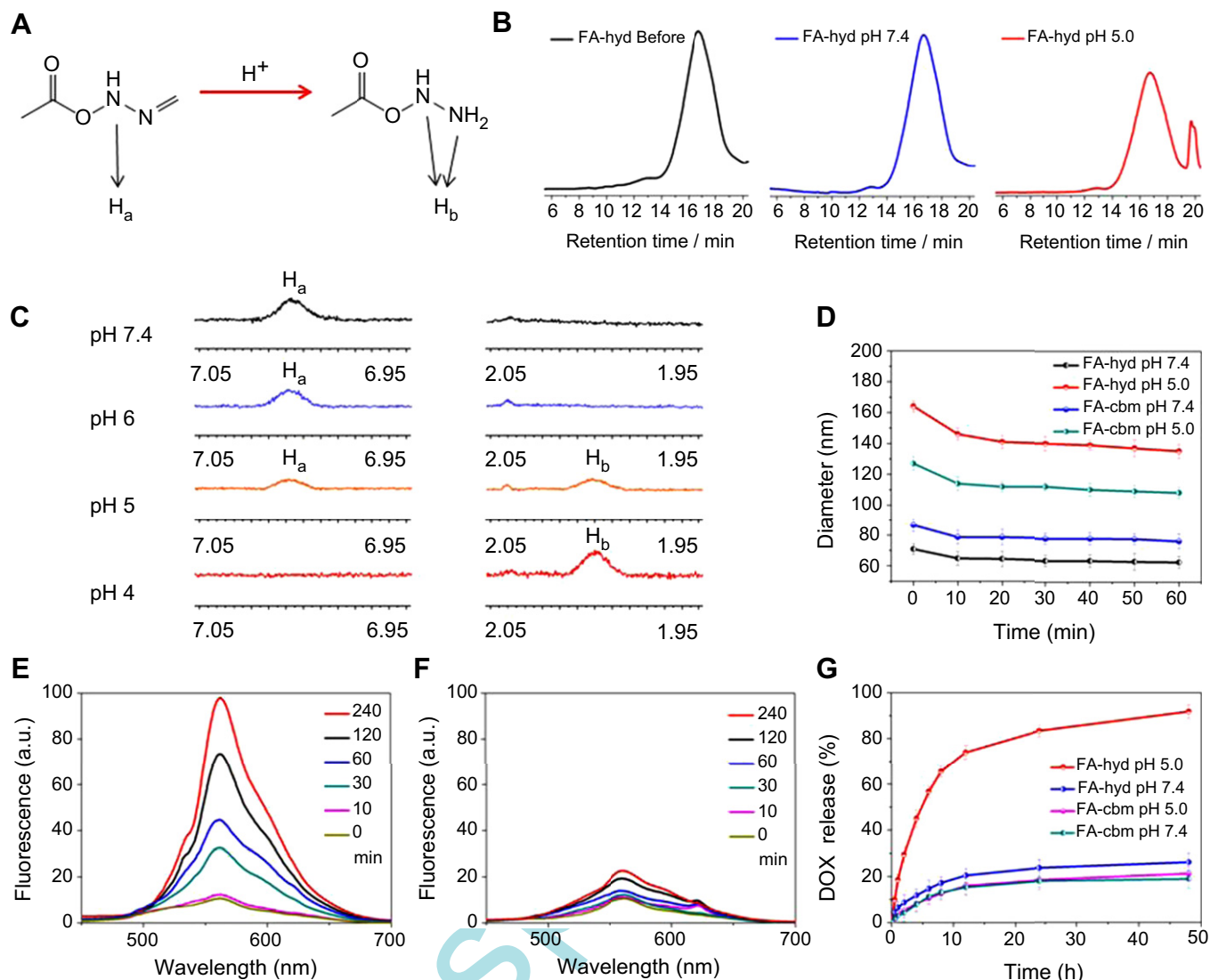
Fig. 2. pH-responsive behaviors and controlled drug release kinetics of DOX-conjugates. Hydrazone bond was broken in the presence of H$^+$ (A). GPC curves of hydrazone bond broken in FA-hyd before and under pH ~ 7.4 or pH ~ 5.0 in DMF (B). ^{1}H NMR spectra of hydrazone bond broken in FA-hyd under pH ~ 7.4, pH ~ 6, pH ~ 5 and pH ~ 4 (C). Size change of the DOX-conjugated micelles at pH 7.4 or at pH 5.0 against time measured by DLS (D). Fluorescence emission spectra of FA-hyd after incubation in acetate buffer solution (ABS) at pH 5.0 (E) or in phosphate buffer solution (PBS) at pH 7.4 (F). In vitro quantitative DOX release from the DOX-conjugated micelles in ABS and PBS, respectively (G). Values in (D) and (G) are means ± SD ($n = 3$).

appeared if FA-hyd was pre-incubated under pH ~ 5.0, which was regarded as the peak of DOX released from FA-hyd (Fig. 2B).

The pH-responsive behavior of the FA-hyd was further investigated by ^{1}H NMR. After the incubation of FA-hyd under different pH conditions for 24 h, the intensity of the peaks at 7.02 ppm of hydrazone protons (H$_a$) decreased at pH 5.0 and even disappeared at pH 4.0 (Fig. 2C). Meanwhile, a new peak at 2.01 ppm of amino groups (H$_b$) appeared at pH 5.0 and increased at pH 4.0. However, the hydrazone bonds in FA-hyd were very stable under pH 7.4 and pH 6.0 for 24 h. These results indicated that the hydrazone bonds in FA-hyd could be broken under endo/lysosomes conditions of cancer cells, while remain stable under normal physiological conditions and in extracellular environment [37].

To investigate the pH-sensitivity of the DOX-conjugated micelles, DLS was used to measure the size change of FA-hyd and FA-cbm micelles against time at pH 7.4 or at pH 5.0, respectively. Due to the protonation of the glycosidic amine of DOX at acidic pH, the size of FA-cbm micelles at pH 5.0 was slightly larger than that at pH 7.4. It was noted that the size of FA-hyd micelles varied more

dramatically along with different pH values and was significantly larger at pH 5.0. This could be ascribed to the protonation of amino group which was generated from the cleavage of the hydrazone bonds (Fig. 2A). All of the micelles became smaller against time due to the release of DOX, while the rate of decrease was faster for FA-hyd micelles at pH 5.0 than other groups, further confirming the pH-sensitivity of the hydrazone bonds (Fig. 2D).

The cleavage of hydrazone linkers of FA-hyd micelles will result in the release of DOX. To demonstrate this, the conjugates with hydrazone linkers were incubated in either acetate buffer solution (ABS) at pH 5.0 or phosphate buffer solution (PBS) at pH 7.4, and the fluorescence emission spectrum at different time intervals was measured. As shown in the Fig. 2E, the DOX fluorescent intensity increased rapidly in a short time at pH 5.0 but almost did not change at pH 7.4 after 4 h incubation (Fig. 2F).

To quantitatively determine the profile of DOX release from the conjugates, the freeze-dried micelles were suspended in either ABS with pH 5.0 or PBS with pH 7.4, and dialyzed at 37 °C for 48 h. As shown in Fig. 2G, 26.17 ± 0.38% of DOX was released from FA-hyd

micelles at pH 7.4. However, 70 ± 4.5% of DOX was released within 10 h when the conjugates with hydrazone linkers were incubated at pH 5.0, indicating the hydrazone bonds are sensitive to the endo/lysosomal pH values. In contrast, the cumulative release of DOX from FA-cbm micelles was 21.16 ± 0.25% at pH 5.0 and 18.89 ± 0.42% at pH 7.4 after 48 h of incubation, indicating pH condition did not significantly affect DOX release from the micelles with a carbamate linker. The result demonstrates that the pH-triggered DOX release profile can be controlled by the hydrazone linker.

3.4. Internalization and intracellular drug release

Confocal laser scanning microscopy (CLSM) analysis was performed for KB cells to further investigate the effects of FA ligands on the cellular uptake and two linkers on the subcellular localization of the DOX-conjugates. As shown in Fig. 3A, KB cells treated with either free DOX or FA-hyd micelles presented a strong DOX fluorescence in the nucleus, while FA-cbm micelles appeared to be entrapped in the endo/lysosomes at 2 h with overlay of yellow fluorescence, and no red fluorescence was observed in the nucleus. This could be attributed to the fact that the carbamate linkers used to conjugate DOX to micelles is hardly cleaved in the acidic compartments such as endo/lysosomes, while the hydrazone linker is broken easily under these conditions. This result was also in good agreement with the pH-responsive behavior of FA-hyd as demonstrated by ^{1}H NMR (Fig. 2C). Besides, the protonation of amino group generated from the cleavage of the hydrazone bond would assist the micelles in escaping from endo/lysosomes (Fig. 3A). In the absence of FA ligands, the DOX fluorescence of KB cells treated with m-hyd micelles was very weak, reflecting the insignificant nonspecific cellular uptake of micelles. The weak fluorescence was also observed for KB cells which were treated firstly with free FA for 0.5 h and followed with FA-hyd micelles, suggesting that pre-incubation with FA ligands effectively blocked FA-hyd micelles to bind to folate receptors on the KB cell surface and thus resulted in a decrease of the receptor-mediated endocytosis [47].
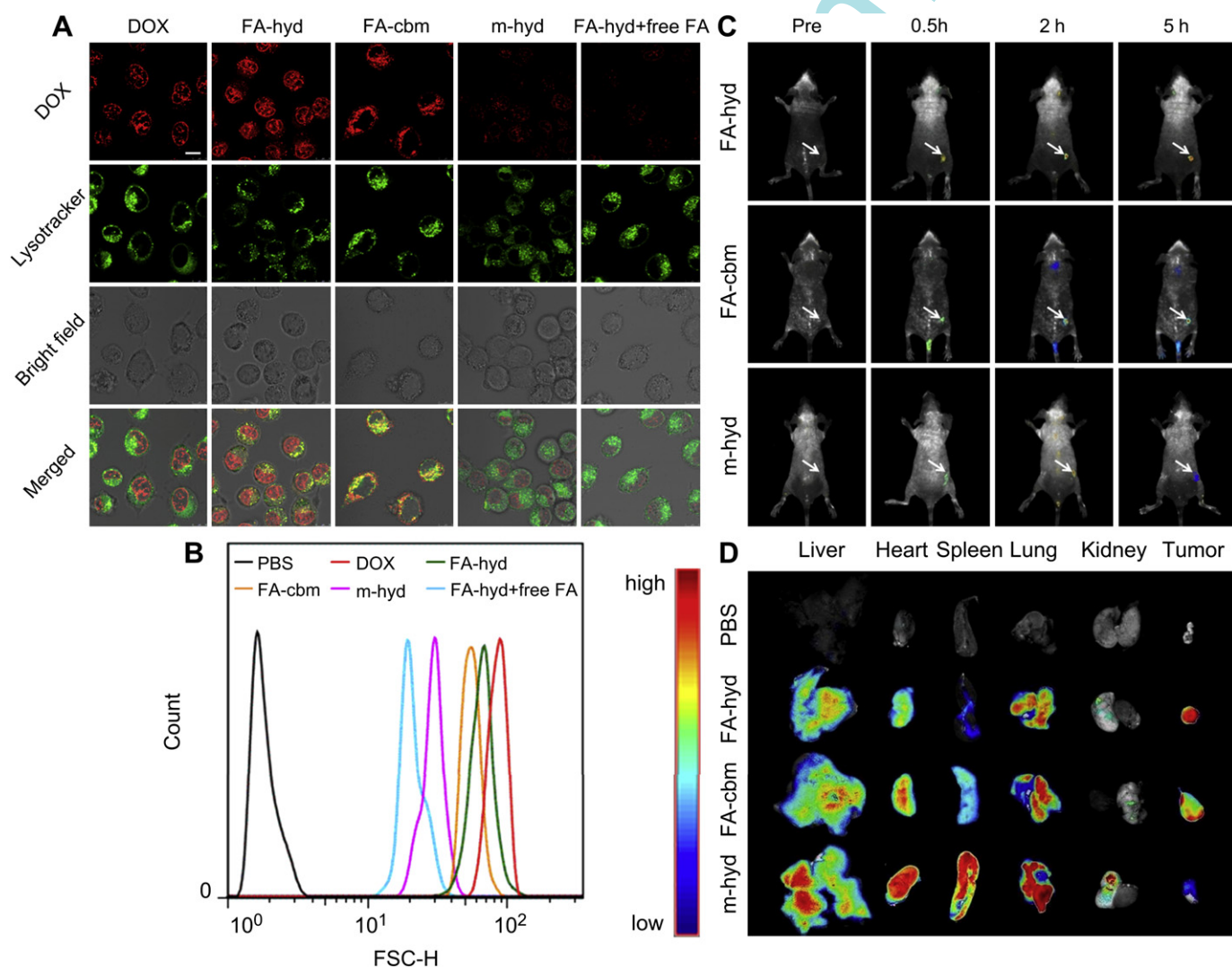
Fig. 3. Confocal laser scanning micrographs of KB cells after incubation with free DOX, FA-hyd, FA-cbm, m-hyd or FA-hyd micelles with a blocking dose of free FA (A). Lysosomes were stained with Lysotracker (green). Cells were incubated for 2 h at 37 °C (DOX-equivalent dose: 5 μg/mL). Yellow color is an indication for localization of DOX (red) in endo/lysosomes (green). (Scale bars, 10 μm). Flow cytometry analysis of KB cells treated with free DOX and DOX-conjugated micelles (all with equivalent DOX concentration of 5 μg/ml), or medium alone (control) for 2 h at 37 °C (B). In vivo DOX fluorescence images showing active tumor accumulation of DOX-conjugated micelles after tail-vein injection into female nude mice bearing the 4T1 xenograft (dose: 5 mg DOX per kg body weight) (C). Ex vivo DOX fluorescence images showing the DOX bio-distribution in female nude mice bearing 4T1 tumor at 5 h postinjection (dose: 5 mg DOX/kg body weight) (D). (For interpretation of the references to color in this figure legend, the reader is referred to the web version of this article.)

The quantitative flow cytometry analysis was then performed for KB cells treated with free DOX and the conjugates at 2 h, and demonstrated that the cellular uptake of FA-hyd micelles was only slightly lower than that of free DOX (Fig. 3B). Cells treated with FA-hyd micelles exhibited a 3 more times cellular uptake higher than cells treated with either m-hyd micelles or FA-blocking micelles. The result also evidenced that folic acid conjugation markedly increased the cellular uptake of micelles by FR-positive cells, and the pH sensitivity of hydrazone linkers facilitated the escape of micelles from the acidic endo/lysosomes.
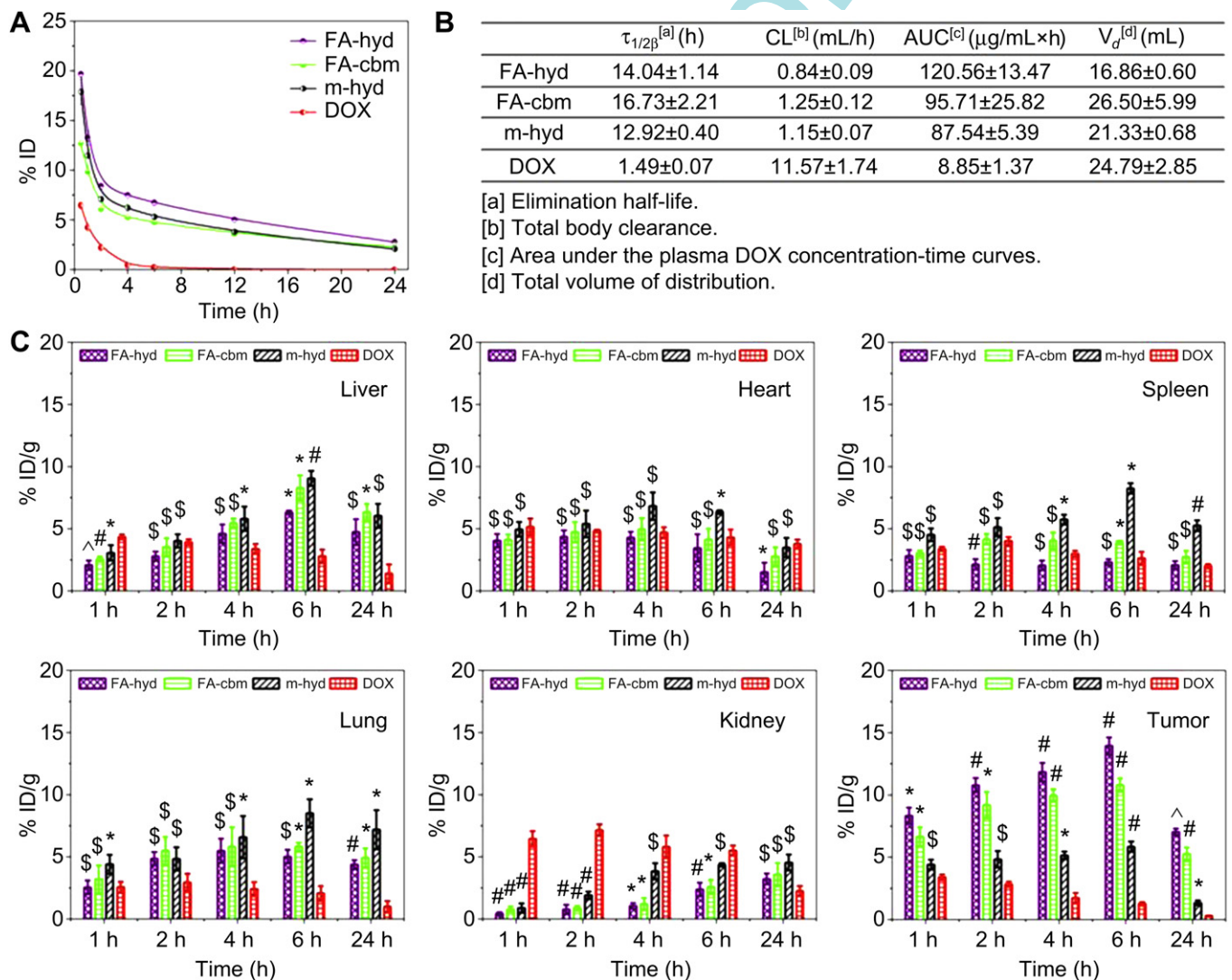
3.5. Biocompatibility evaluation

The biocompatibility of the blank micelles with red blood cells was examined by a hemolytic test. As shown in Fig. S5A and B, the coagulation factors (FVIII, FIX and FXI) and thrombin generation (TAT) were not activated by FA-PECL micelles. This is a proof to confirm that the blank micelles possess good blood compatibility. Co-culture of osteoblasts (OB), A549 and KB cells with FA-PECL micelles demonstrated that blank micelles did not present significant cytotoxicity at the tested concentration ranging from 10 to

100 μg/mL (Supporting information, Fig. S6). The cytotoxic activity of DOX-conjugated micelles against KB (FR+) and A549 (FR−) cells was evaluated (Supporting information, Fig. S7). In KB cells, FA-hyd micelles were the most effective treatment (IC$_{50}$, 0.51 μg/mL). This formulation was around 3 times cytotoxicity than free DOX (IC$_{50}$, 1.51 μg/mL), 14 times more cytotoxic than the m-hyd micelles (IC$_{50}$, 7.51 μg/mL) and the FA-blocking micelles (IC$_{50}$, 7.25 μg/mL). The IC$_{50}$ value of free DOX for KB cells was comparatively higher than other cell lines, indicating that FR-positive cells are more resistant to the treatment of DOX [48].

3.6. In vivo and ex vivo DOX fluorescence imaging

To directly visualize the transfer of the micelles in vivo, we injected the different groups of DOX-conjugated micelles to nude mice which are bearing 4T1 tumor, and then monitored the fluorescence intensity of DOX at different sites of body and at different time intervals by ex vivo imaging. Compared to other groups, FA-hyd micelles were accumulated at the tumor site more obviously at all tested times as shown in Fig. 3C. Ex vivo imaging showed that the m-hyd micelles were distributed to the normal tissues rather

	$\tau_{1/2\beta}$[a] (h)	CL[b] (mL/h)	AUC[c] (μg/mL×h)	V_d[d] (mL)
FA-hyd	14.04±1.14	0.84±0.09	120.56±13.47	16.86±0.60
FA-cbm	16.73±2.21	1.25±0.12	95.71±25.82	26.50±5.99
m-hyd	12.92±0.40	1.15±0.07	87.54±5.39	21.33±0.68
DOX	1.49±0.07	11.57±1.74	8.85±1.37	24.79±2.85

[a] Elimination half-life.
[b] Total body clearance.
[c] Area under the plasma DOX concentration-time curves.
[d] Total volume of distribution.

Fig. 4. Pharmacokinetic profiles of total DOX after i.v. injection of DOX solution and DOX-conjugated micelles at a dose of 5 mg DOX-equiv./kg ($n = 3$) (A). Pharmacokinetic parameters of free DOX and DOX-conjugated micelles (B). Distribution profiles of total DOX in tissues after i.v. injection of DOX solution and DOX-conjugated micelles at a dose of 5 mg DOX-equiv./kg ($n = 3$) (C). $, not significant; *, $P < 0.05$; #, $P < 0.01$; ˆ, $P < 0.001$, as compared with DOX solution at the same time point (t-test using SPSS, 17.0).

than to the tumors. In contrast, a little of the targeted micelles were accumulated at normal tissues, but much more were enriched at tumor sites. And the FA-hyd group displayed the strongest fluorescence intensity in the tumor than other groups (Fig. 3D). These results suggested that the drug delivery system with the FA-functionalized micelles presented much better specificity to target tumor in vivo.

3.7. Evaluation of pharmacokinetics and biodistribution of DOX in vivo

To evaluate pharmacokinetic of DOX in vivo, we treated BALB/c mice with a single intravenous injection of free DOX and DOX-conjugates (5 mg/kg DOX equiv), collected plasma at different time intervals, and then determined the level of DOX by fluorescence spectroscopy. From the blood clearance curves obtained for free DOX, FA-hyd, FA-cbm and m-hyd (Fig. 4A), and the pharmacokinetic parameters $\tau_{1/2\beta}$ (h), CL (mL/h), AUC (μg/mL × h) and V_d (mL) obtained by fitting the blood drug concentration versus time using a two-compartment model (Fig. 4B), we can find that compared to the free DOX, the elimination of DOX from the blood was significantly slower when it was conjugated to the micelles. DOX conjugates with FA-cbm micelles displayed a slightly longer half-time than others conjugated with a hydrazone linkage, which may be partially due to the stronger stability of the carbamate linkage. However, the AUC for the FA-hyd conjugates (120.56 ± 13.47 μg/mL × h) was greater than the FA-cbm (95.71 ± 25.82), which resulted in a corresponding decrease in CL for FA-hyd (0.84 ± 0.09) compared to FA-cbm (1.25 ± 0.12). Similarly, V_d for FA-hyd (16.86 ± 0.60) was remarkably lower than that for FA-cbm (26.50 ± 5.99).

We then investigated if the bio-distribution of DOX in mouse body was changed after being conjugated with micelles. As shown
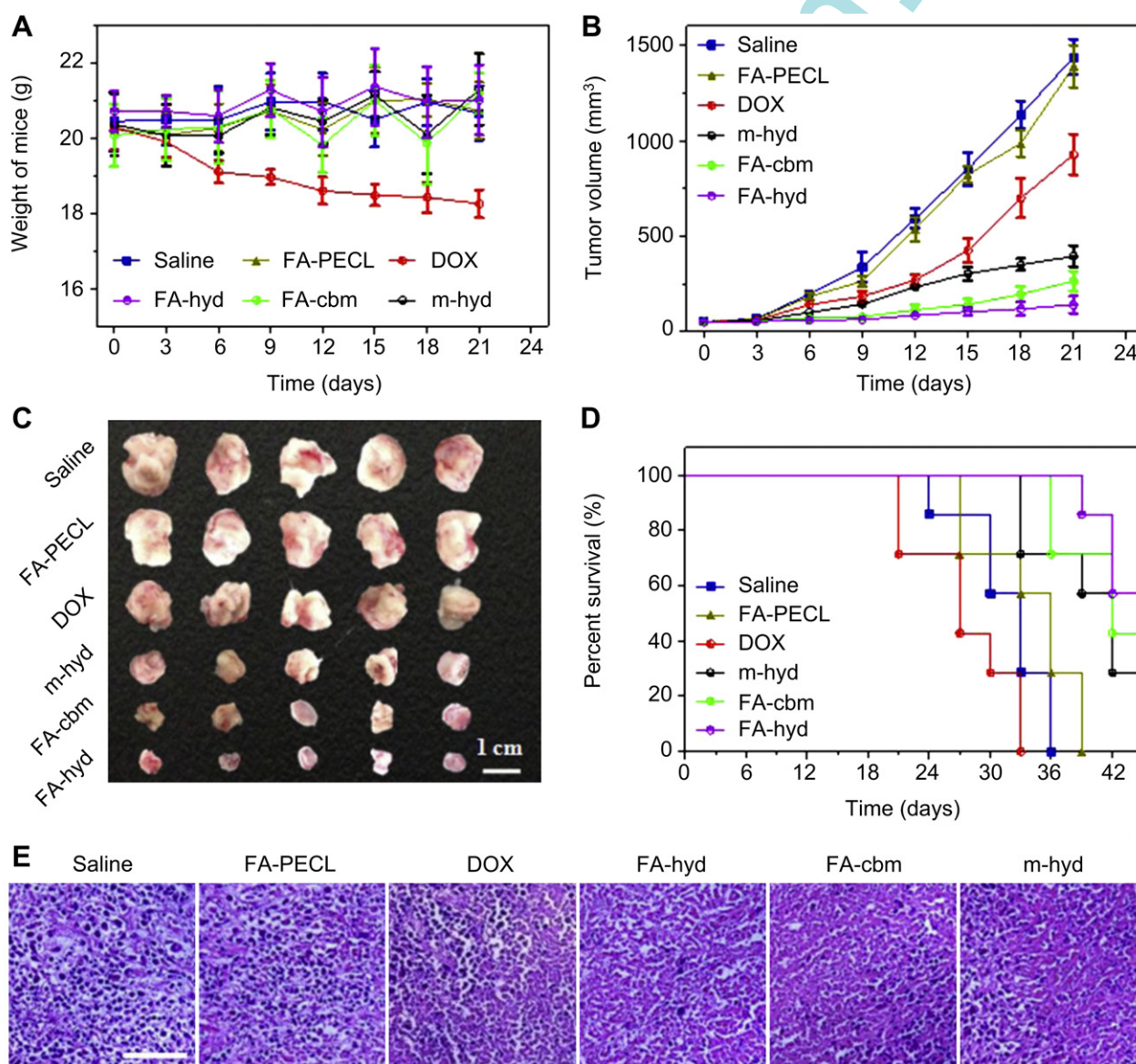
Fig. 5. In vivo antitumor effect and systemic toxicity of free DOX and DOX-conjugated micelles injected into BALB/c mice at a dose of 5 mg/kg. Body weight changes of 4T1 tumor bearing mice ($n = 7$) (A). Tumor volume changes of different treatment groups ($n = 7$) (B). Excised 4T1 solid tumors from different treatment groups at the 21st day (C). Survival curves of mice with 4T1 breast tumors ($n = 7$) (D). H&E stained 4T1 tumor sections (21 days after the first treatment) (E). Nuclei were stained blue while extracellular matrix and cytoplasm were stained red (Scale bars, 50 μm). Values in (A) and (B) are means ± SD. (For interpretation of the references to color in this figure legend, the reader is referred to the web version of this article.)

in Fig. 4C, DOX was typically accumulated in liver, heart, spleen, lung, kidneys and tumor after intravenous injection of either free DOX or DOX-conjugates. Compared to free DOX, accumulation of DOX-conjugates greatly increased in the tumor through the EPR effect. According to previous work, the effective DOX level in tumor tissue is 6.4 μg/g [49]. Herein, the level of DOX could be above 6 μg/g in tumor and be sustained for 24 h in folic acid-attached groups and only 6 h in the m-hyd group. Longer exposure to DOX with the effective concentration also leads to a greater antitumor efficacy.

Besides, extensive accumulation of total DOX was observed in liver, spleen and lung for the m-hyd without targeting moiety; however, with the attachment of folic acid ligands the accumulation in these normal tissues decreased but increased in tumor. Similar to results of ex vivo DOX fluorescence imaging (Fig. 3C), the FA-hyd showed less reticuloendothelial system (RES) uptake and more tumor accumulation than the FA-cbm.

3.8. In vivo antitumor effect

Fig. 5 illustrates the toxicity and antitumor effect of various formulations after being applied to the BALB/c mice bearing 4T1 tumor. Measurements on survival rate (Fig. 5A) and body weight (Fig. 5B) showed that DOX-conjugated micelles possessed better safety to body than free DOX. Meanwhile, DOX-conjugated micelles, especially the FA-hyd micelles showed a better antitumor effect than that of free DOX (Fig. 5C and D). These results indicated that the conjugation of DOX on the hydrophobic core of the micelles remarkably reduced the exposure of DOX to normal tissues and thus decreased the toxicity of chemotherapeutics.

In situ histological study was supportive of the excellent therapeutic effect of the targeting and pH-sensitive micelles. When the FA-hyd micelles were administered, a minimum number of tumor cells were shown in hematoxylin and eosin (H&E) staining (Fig. 5E). Thus, the FA-hyd micelles were regarded as the most effective and safe formulation in vivo. Firstly, EPR effect increased the accumulation of micelles to the tumor site [15], and FA attached on the micelles actively targeted tumor cells and augmented the internalization of micelles [25]. Secondly, the hydrazone linkers effectively helped the FA-hyd micelles to escape from the endo/lysosomes, which resulted in the nucleus delivery of DOX and finally induced the apoptosis of tumor cells.

4. Conclusions

In this study, we develop a nanomedicine system for intelligent anticancer drug delivery in which polymeric-drug conjugated micelles are equipped with a folic acid for the actively tumor targeting and a pH-sensitive hydrazone linkage for the controlled drug release. The nanocarriers circulate for long periods in blood and selectively accumulate in tumor sites. They are preferentially cleavable in neoplastic tissues and stable in blood plasma, thus the triggered release of the payloads is realized only under acidic tumor environment. Importantly, the nanocarriers can escape from the endo/lysosomes of tumor cells and ensure the nuclear delivery of anticancer drug, which greatly improve the therapeutic efficiency and decrease the drug toxicity. Therefore, the study provides a facile engineered strategy towards the design and fabrication of multifunctional nanocarriers for effective and safe cancer therapy.

Appendix A. Supplementary data

Supplementary data related to this article can be found at http://dx.doi.org/10.1016/j.biomaterials.2013.02.071.

References

[1] Ferrari M. Cancer nanotechnology: opportunities and challenges. Nat Rev Cancer 2005;5:161–71.
[2] Duncan R. The dawning era of polymer. Nat Rev Drug Discov 2003;2:347–60.
[3] Peer D, Karp JM, Hong S, Farokhzad OC, Margalit R, Langer R. Nanocarriers as an emerging platform for cancer therapy. Nat Nanotechnol 2007;2:751–60.
[4] Lammers T, Aime S, Hennink WE, Storm G, Kiessling F. Theranostic nanomedicine. Acc Chem Res 2011;44:1029–38.
[5] Xiao Z, Valencia PM, Radovic-Moreno AF, Farokhzad OC. Targeted polymeric therapeutic nanoparticles: design, development and clinical translation. Chem Soc Rev 2012;41:2971–3010.
[6] Koo H, Huh MS, Sun IC, Yuk SH, Choi K, Kim K, et al. In vivo targeted delivery of nanoparticles for theranosis. Acc Chem Res 2011;44:1018–28.
[7] Bae Y, Fukushima S, Harada A, Kataoka K. Design of environment-sensitive supramolecular assemblies for intracellular drug delivery: polymeric micelles that are responsive to intracellular pH change. Angew Chem Int Ed 2003;42:4640–3.
[8] Hubbell JA, Chilkoti A. Nanomaterials for drug delivery. Science 2012;337: 303–5.
[9] Farokhzad OC, Langer R. Impact of nanotechnology on drug delivery. ACS Nano 2009;3:16–20.
[10] Shi JJ, Votruba AR, Farokhzad OC, Langer R. Nanotechnology in drug delivery and tissue engineering: from discovery to applications. Nano Lett 2010;10: 3223–30.
[11] Petros RA, DeSimone JM. Strategies in the design of nanoparticles for therapeutic applications. Nat Rev Drug Discov 2010;9(8):615–27.
[12] Barreto JA, Malley OW, Kubeil M, Graham B, Stephan H, Spiccia L. Nanomaterials: applications in cancer imaging and therapy. Adv Mater 2011;23: H18–40.
[13] Cabral H, Matsumoto Y, Mizuno K, Chen Q, Murakami M, Kimura M, et al. Accumulation of sub-100 nm polymeric micelles in poorly permeable tumours depends on size. Nat Nanotechnol 2011;6:815–23.
[14] Matsumura Y, Maeda H. A new concept for macromolecular therapeutics in cancer chemotherapy: mechanism of tumoritropic accumulation of proteins and the antitumor agent smancs. Cancer Res 1986;46:6387–92.
[15] Maeda H, Wu J, Sawa T, Matsumura Y, Hori K. Tumor vascular permeability and the EPR effect in macromolecular therapeutics: a review. J Control Release 2000;65:271–84.
[16] Adair JH, Parette MP, Altınoğlu Eİ, Kester M. Nanoparticulate alternatives for drug delivery. ACS Nano 2010;4:4967–70.
[17] Rapoport N. Physical stimuli-responsive polymeric micelles for anti-cancer drug delivery. Prog Polym Sci 2007;32:962–90.
[18] Gottesman MM, Fojo T, Bates SE. Multidrug resistance in cancer: role of ATP-dependent transporters. Nat Rev Cancer 2002;2:48–58.
[19] Nasongkla N, Shuai XT, Ai H, Weinberg BD, Pink J, Boothman DA, et al. cRGD-functionalized polymer micelles for targeted doxorubicin delivery. Angew Chem 2004;116:6483–7.
[20] Kim J, Lee JE, Lee SH, Yu JH, Lee JH, Park TG, et al. Designed fabrication of a multifunctional polymer nanomedical platform for simultaneous cancer-targeted imaging and magnetically guided drug delivery. Adv Mater 2008;20:478–83.
[21] Daniels TR, Delgado T, Rodriguez JA, Helguera G, Penichet ML. The transferrin receptor part I: biology and targeting with cytotoxic antibodies for the treatment of cancer. Clin Immunol 2006;121:144–58.
[22] Torchilin VP, Lukyanov AN, Gao Z, Papahadjopoulos-Sternberg B. Immunomicelles: targeted pharmaceutical carriers for poorly soluble drugs. Proc Natl Acad Sci USA 2003;100:6039–44.
[23] Lammers T, Kiessling F, Hennink WE, Storm G. Drug targeting to tumors: principles, pitfalls and (pre-) clinical progress. J Control Release 2012;161: 175–87.
[24] Tanner P, Baumann P, Enea R, Onaca O, Palivan C, Meier W. Polymeric vesicles: from drug carriers to nanoreactors and artificial organelles. Acc Chem Res 2011;44:1039–49.
[25] Low PS, Henne WA, Doorneweerd DD. Discovery and development of folic-acid-based receptor targeting for imaging and therapy of cancer and inflammatory diseases. Acc Chem Res 2007;41:120–9.
[26] Ashley CE, Carnes EC, Phillips GK, Padilla D, Durfee PN, Brown PA, et al. The targeted delivery of multicomponent cargos to cancer cells by nanoporous particle-supported lipid bilayers. Nat Mater 2011;10:389–97.
[27] Wang WW, Cheng D, Gong FM, Miao XM, Shuai XT. Design of multifunctional micelle for tumor-targeted intracellular drug release and fluorescent imaging. Adv Mater 2012;24:115–20.

[28] Nori A, Kopeček J. Intracellular targeting of polymer-bound drugs for cancer chemotherapy. Adv Drug Deliver Rev 2005;57:609–36.

[29] Loomis K, McNeeley K, Bellamkonda RV. Nanoparticles with targeting, triggered release, and imaging functionality for cancer applications. Soft Matter 2010;7:839–56.

[30] Xiong XB, Falamarzian A, Garg SM, Lavasanifar A. Engineering of amphiphilic block copolymers for polymeric micellar drug and gene delivery. J Control Release 2011;155:248–61.

[31] Zhou KJ, Wang YG, Huang XN, Luby-Phelps K, Sumer BD, Gao JM. Tunable, ultrasensitive pH-responsive nanoparticles targeting specific endocytic organelles in living cells. Angew Chem Int Ed 2011;50:6109–14.

[32] Du JZ, Sun TM, Song WJ, Wu J, Wang J. A tumor-acidity-activated charge-conversional nanogel as an intelligent vehicle for promoted tumoral-cell uptake and drug delivery. Angew Chem Int Ed 2010;49:3621–6.

[33] Du JZ, Du XJ, Mao CQ, Wang J. Tailor-made dual pH-sensitive polymer-doxorubicin nanoparticles for efficient anticancer drug delivery. J Am Chem Soc 2011;133:17560–3.

[34] Zhou KJ, Liu HM, Zhang SR, Huang XN, Wang YG, Huang G, et al. Multicolored pH-tunable and activatable fluorescence nanoplatform responsive to physiologic pH stimuli. J Am Chem Soc 2012;134:7803–11.

[35] Wang F, Wang YC, Dou S, Xiong MH, Sun TM, Wang J. Doxorubicin-tethered responsive gold nanoparticles facilitate intracellular drug delivery for overcoming multidrug resistance in cancer cells. ACS Nano 2011;5:3679–92.

[36] Lim EK, Huh YM, Yang J, Lee K, Suh JS, Haam S. pH-triggered drug-releasing magnetic nanoparticles for cancer therapy guided by molecular imaging by MRI. Adv Mater 2011;23:2436–42.

[37] Martin GR, Jain RK. Noninvasive measurement of interstitial pH profiles in normal and neoplastic tissue using fluorescence ratio imaging microscopy. Cancer Res 1994;54:5670–4.

[38] Hubbell JA. Enhancing drug function. Science 2003;300:595–6.

[39] Fleige E, Quadir MA, Haag R. Stimuli-responsive polymeric nanocarriers for the controlled transport of active compounds: concepts and applications. Adv Drug Deliver Rev 2012;15:866–84.

[40] Khandare J, Minko T. Polymer-drug conjugates: progress in polymeric prodrugs. Prog Polym Sci 2006;31:359–97.

[41] Pasut G, Veronese FM. Polymer-drug conjugation, recent achievements and general strategies. Prog Polym Sci 2007;32:933–61.

[42] Duncan R. Polymer conjugates as anticancer nanomedicines. Nat Rev Cancer 2006;6:688–701.

[43] Zhang W, Shi Y, Chen Y, Ye J, Sha XY, Fang XL. Multifunctional Pluronic P123/F127 mixed polymeric micelles loaded with paclitaxel for the treatment of multidrug resistant tumors. Biomaterials 2011;32:2894–906.

[44] Batrakova EV, Vinogradov SV, Robinson SM, Niehoff ML, Banks WA, Kabanov AV. Polypeptide point modifications with fatty acid and amphiphilic block copolymers for enhanced brain delivery. Bioconjug Chem 2005;16:793–802.

[45] Hu XL, Liu S, Huang YB, Chen XS, Jing XB. Biodegradable block copolymer-doxorubicin conjugates via different linkages: preparation, characterization, and in vitro evaluation. Biomacromolecules 2010;11:2094–102.

[46] Geng J, Li K, Ding D, Zhang X, Qin W, Liu J, et al. Lipid-PEG-folate encapsulated nanoparticles with aggregation induced emission characteristics: cellular uptake mechanism and two-photon fluorescence imaging. Small 2012;8:3655–63.

[47] Bharali DJ, Lucey DW, Jayakumar H, Pudavar HE, Prasad PN. Folate-receptor-mediated delivery of InP quantum dots for bioimaging using confocal and two-photon microscopy. J Am Chem Soc 2005;127:11364–71.

[48] Emilienne Soma C, Dubernet C, Bentolila D, Benita S, Couvreur P. Reversion of multidrug resistance by co-encapsulation of doxorubicin and cyclosporin A in polyalkylcyanoacrylate nanoparticles. Biomaterials 2000;21:1–7.

[49] Weinberg BD, Ai H, Blanco E, Anderson JM, Gao J. Antitumor efficacy and local distribution of doxorubicin via intratumoral delivery from polymer millirods. J Biomed Mater Res Part A 2007;81:161–70.